ELSEVIER

Polymer 41 (2000) 4267–4279

polymer

Phase structure, composition and orientation of PC/PSAN blends studied by Raman spectroscopy, confocal Raman imaging spectroscopy and polarised PA-FTIR spectroscopy

P. Schmidt[a,*], J. Kolařík[a], F. Lednický[a], J. Dybal[a], J.M. Lagarón[b], J.M. Pastor[b]

[a]*Institute of Macromolecular Chemistry, Academy of Sciences of the Czech Republic, Heyrovský Sq. 2, 162 06 Prague, Czech Republic*
[b]*Department of Condensed Matter/E.T.S.I.I., University of Valladolid, 47011 Valladolid, Spain*

Received 4 January 1999; accepted 30 July 1999

Abstract

Polycarbonate(PC)/ poly(styrene-*co*-acrylonitrile)(PSAN) blends were investigated by Raman and confocal Raman imaging spectroscopy, revealing the existence of two-phase (PC-rich and PSAN-rich) microdomain structure. This structure is coarser in blends with comparable component contents. During cold drawing the microdomains are strongly extended. As follows from polarised photoacoustic FTIR spectroscopy, a substantial orientation of PC chains occurs, as opposed to PSAN chains which orient only slightly.

Keywords: Polycarbonate/poly(styrene-*co*-acrylonitrile) blends; Microstructure; Chain orientation

1. Introduction

Bisphenol A polycarbonate (PC) attracts much attention in materials research because of its outstanding mechanical properties. Blends of PC with other polymers have been prepared and extensively investigated (see citations in Refs. [1–3]). It is known that mechanical properties of polymer blends are closely related to their composition, phase structure, interface adhesion and molecular orientation. PC and poly(styrene-*co*-acrylonitrile) (PSAN) belong to the class of partly miscible polymers forming heterogeneous blends with a good interface adhesion at the formed interphases, which ensures a good stress transmission between constituents during deformation up to fracture.

The composition of the PC-rich and PSAN-rich conjugate phases was calculated from the DSC measurements of glass transition temperatures of parent polymers and blends [1]. The PC-rich and PSAN-rich domains were morphologically distinguished by transmission electron microscopy (TEM) and/or scanning tunnelling electron microscopy (STEM) after staining the ultra-thin sections of these blends with osmium or ruthenium [1–3].

The capabilities of confocal Raman imaging spectroscopy and photoacoustic Fourier transform infrared (PA-FTIR) spectroscopy for the investigation of various polymer systems were demonstrated e.g. in Refs. [4,5]. The objective of this paper is the application of these methods to further characterise the PC/PSAN blends, i.e., to confront spectral images of the phase structure with morphological formations seen in TEM and STEM micrographs [1–3]. Furthermore, we aim to determine spectroscopically the local polymer composition of the conjugate phases in microdomains and to compare it with the data calculated from glass transition temperatures [1]. Finally, we estimate the changes in chain orientation caused by plastic deformation and by the following annealing.

2. Experimental

2.1. Samples

Bisphenol A polycarbonate (PC) was Sinvet 251, (ENI, Italy). Poly(styrene-*co*-acrylonitrile) (PSAN) containing 24 wt% of acrylonitrile was Kostil AF 600 (ENI, Italy). Samples of PC, PSAN and the PC/PSAN blends of mass ratios 20/80, 30/70, 40/60, 50/50, 60/40, 70/30, 80/20 were mixed and injection moulded as described previously [3]. Dumbbell-shape specimens were drawn at room temperature up to fracture at the strain rate of 5% min^{-1}. During straining, PC exhibited plastic deformation and could be drawn up to about 170%. The attained elongation decreased

* Corresponding author. Tel.: +420-2-20403111; fax.: +420-2-367981.
E-mail address: schmidt@imc.cas.cz (P. Schmidt).

0032-3861/00/$ - see front matter
PII: S0032-3861(99)00551-0

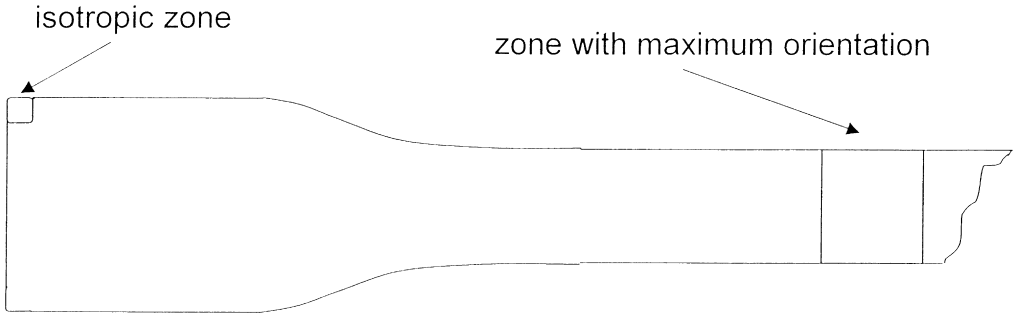

Fig. 1. Scheme of the PC/PSAN dumbbell after plastic deformation and localisation of the measured areas. Isotropic zone and zone with maximum orientation are marked.

with the percentage of PSAN in the blends [3]: the PC/PSAN = 30/70 specimen broke after yielding, the 20/80 blend and PSAN were brittle. The interference effects of visible polarised light at very low magnifications revealed the lowest material orientation due to injection moulding in the corners of the test pieces distant from the inlet, as schematically shown in Fig. 1. In this way, both an isotropic zone and the parts with the maximum orientation of the material were optically identified in each of the test pieces.

For the study of gradual disorientation of the material, the specimens were annealed in a vacuum oven for 20 h.

2.2. Techniques

Macro-Raman measurements were performed on a Bruker spectrometer IFS 55 equipped with a Raman module FRA 106 at 8 cm^{-1} resolution. Spectra were obtained by using a 1064 nm diode-pumped Nd:YAG laser radiating 500 mW at the sample. The samples were measured as powders obtained by filing the material; the powders were stamped into depressions in aluminium discs. The spectra did not depend on the orientation of the samples with respect to the polarisation plane of the laser beam.

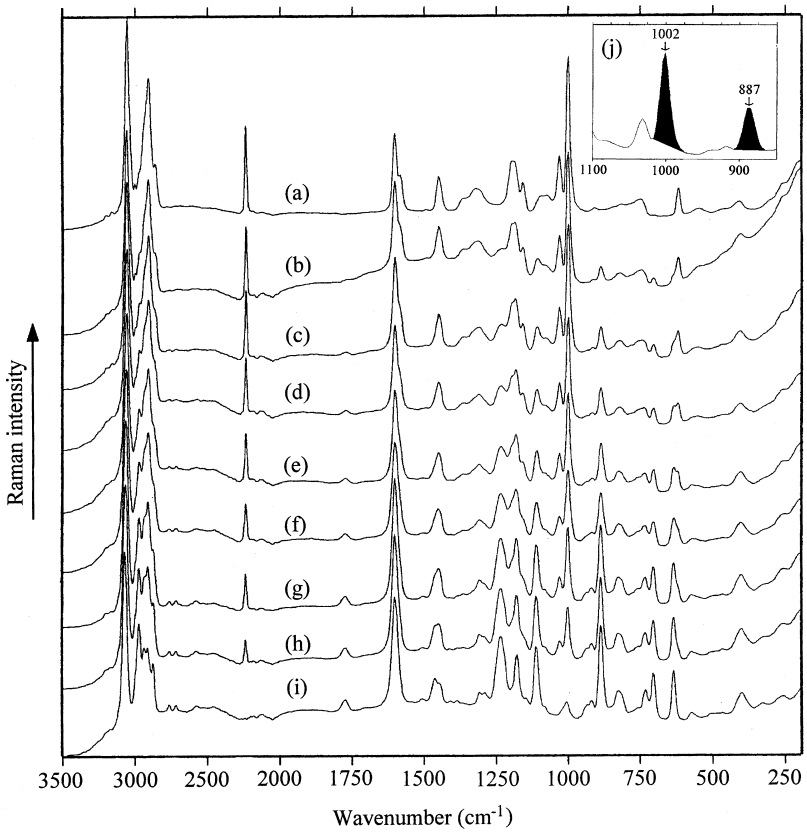

Fig. 2. Macro-Raman spectra of PC/PSAN powders with various compositions. PC/PSAN : (a) 0/100; (b) 20/80; (c) 30/70; (d) 40/60; (e) 50/50; (f) 60/40; (g) 70/30; (h) 80/20; and (i) 100/0. Curve (j) is a magnified part of curve (e), the black areas were used for the formation of images and line profiles and for the determination of concentrations.

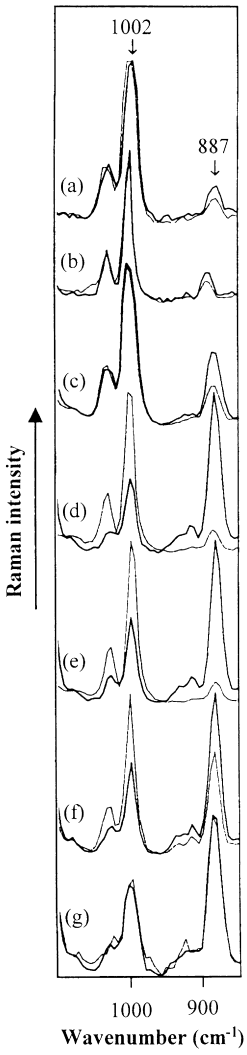

Fig. 3. Micro-Raman spectra with the maximum (—) and with the minimum (···) relative intensity of PC band (887 cm^{-1}) chosen from the 400 measurements of the $5 \times 5\ \mu m^2$ isotropic regions of the respective PC/PSAN specimen. PC/PSAN equals: (a) 20/80; (b) 30/70; (c) 40/60; (d) 50/50; (e) 60/40; (f) 70/30; and (g) 80/20.

A confocal micro-Raman LABRAM equipment from Dilor S.A. (Lille, France) was used for *Raman confocal measurements* and point-by-point mapping [6,7]. This equipment uses a He–Ne laser beam operating at 632 nm which supplies ca 16 mW at the sample surface. The scattered light was detected with a CCD camera. Combination of 100× or 10× objectives, several pinhole apertures (normally 100 μm) and 300 grooves mm^{-1} grating were used. The spectral resolution was 8 cm^{-1}. Point-by-point measurements were carried out using a motorised scanning stage controlled by the computer software LABSPEC (Dilor S.A.). The distance between points in the images and line profiles was usually 0.25 μm. Spectral line profiles and area images of the samples were composed from the measured sets of spectra using the software LABSPEC. They reflect the intensity ratio of two selected Raman bands as a function of the position of the measured region on the sample. Most confocal Raman measurements were carried out in the isotropic zone of the material; oriented parts of some specimens were also measured. The cut surfaces of isotropic samples or of the samples with selected orientation were prepared from the centre of the dumbbell by ultra-thin sectioning, which is the technique used in sample preparation for electron microscopy.

PA-FTIR measurements were performed with an IR spectrometer Bruker IFS66v/S using the MTEC 200 photoacoustic cell (Ames, Iowa). The specimens were cut from the drawn parts of the material with a thickness of 3–4 mm, to fit into the cell holder. After inserting the test piece, the cell was flushed with He for at least l h before the beginning of the measurement. The resolution was 4 cm^{-1}. A carbon black standard was used as reference. The spectra were measured with a mirror frequency of 5 kHz, 1800 scans being accumulated. The direction of the specimen orientation coincided with the plane of the IR beam passing through the photoacoustic cell. For the polarisation of IR radiation, a KRS-5 wire grid polariser (SPECAC) was placed immediately behind the source. Two successive measurements, with parallel (∥) and with perpendicular (⊥) polarisation of the electric vector with respect to the direction of sample deformation, were performed.

Comparative transmittance FTIR measurements were performed with films evaporated from $CHCl_3$ solution on KBr windows, at spectral resolution of 2 cm^{-1}.

3. Results and discussion

3.1. Raman imaging of the microstructure of PC/PSAN *blends*

The macro-Raman spectra characterising the mean composition of PC/PSAN blends for the weight ratios 0/100, 20/80, 30/70, 40/60, 50/50, 60/40, 70/30, 80/20 and 100/0, are shown in Fig. 2. From the Raman spectra of the mixtures of PC and PSAN, two bands at 887 and 1002 cm^{-1} were selected as the most characteristic of PC and PSAN, respectively. For the determination of intensities both in the macro-Raman and in the micro-Raman spectra and for the construction of the composition images and composition line profiles, the areas under the bands (spanning about 50 cm^{-1}) were utilised (see Fig. 2). Macro measurements are not affected by the existence of microdomains as the sample areas measured are much larger.

The confocal micro-Raman results from the isotropic zones were sampled, mapping, point-by-point, the $5 \times 5\ \mu m^2$ squares in steps of 0.25 μm with an 100× objective magnification, so that 400 spectra were obtained. From these, a pair of spectra with the maximum and with the minimum intensities of the PC bands was selected for each specimen. The results of such selection are shown in Fig. 3. Great differences can be seen between the maximum

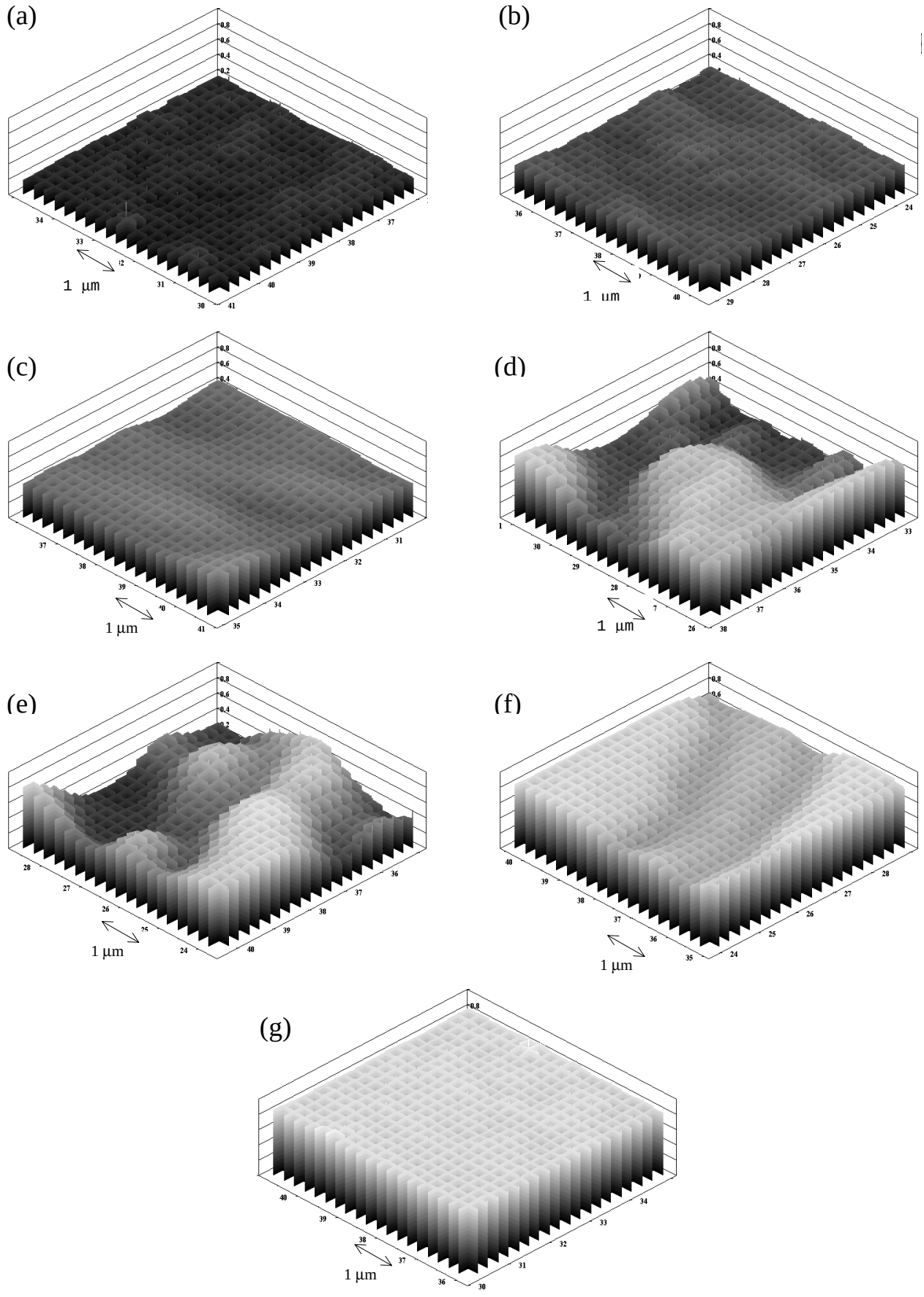
(a)
1 µm
(b)
1 µm
(c)
1 µm
(d)
1 µm
(e)
1 µm
(f)
1 µm
(g)
1 µm

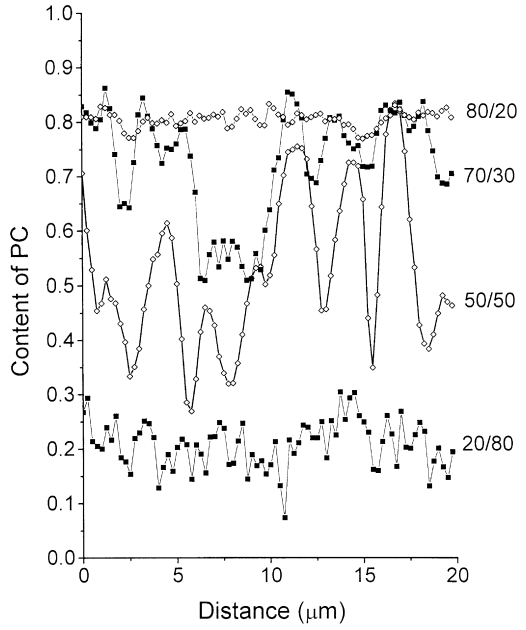

Fig. 5. Spectral composition line profiles of the isotropic PC/PSAN blends of various compositions. The scales of the vertical axis correspond to the values of c_{PC} calculated according to Eq. (1) for each measured point of the respective specimen.

and the minimum for the specimens with comparable contents of PC and PSAN; the differences are much smaller if one of the components highly prevails.

For each specimen, composition images were constructed from the mentioned 400 spectra (see Fig. 4). Similarly, lines typically 20 μm long were scanned to obtain the composition profiles, for which 80 spectra were needed (see Fig. 5). Thus, the phase structures consisting of the domains rich in PC or in PSAN could be visualised.

As follows from the three-dimensional (3D) representation of the images of the measured specimens shown in Fig. 4 (the isotropic zones), the size and shape of the PC-rich and PSAN-rich domains depend on the total blend composition. The two-phase domain structure appears to be coarser for the 60/40, 50/50 and 70/30 samples and also the differences in the domain composition are expressed here more clearly; the structure is finer for the 80/20, 20/80, 30/70 and 40/60 PC/PSAN blends, the differences in the composition appearing more blurred. In the isotropic zones, isometric domains prevail.

The spectral composition line profiles for the isotropic PC/PSAN specimens (some of them shown in Fig. 5) offer results similar to those found for the spectral composition images, i.e. coarser grain structure and better expressed differences in concentrations for the 60/40, 50/50 and 70/30 PC/PSAN blends. For some domains, diameters larger than 2 μm can be found. Approximate mean values of the domain diameter for different PC/PSAN blends as obtained for each sample from the count of maxima and minima of the line profiles are plotted in Fig. 6. They reach 1.1 μm for the 50/50 PC/PSAN blend.

The dimensions of coarse structure domains in the phase inversion interval [3] (PC/PSAN = 50/50, 60/40) are comparable with the structure observed by electron microscopy. Very fine structures, observed in the samples with majority of one component, are obviously blurred because of the lower resolution of the micro-Raman imaging. Nevertheless, a 3D representation of another 50/50 PS/PSAN isotropic zone in Fig. 7a together with a magnified 2D representation of a part of the image in Fig. 7b, reveals the possibility of a more complex compositional structure of the material: inside a PC-rich domain, some very small PSAN-rich domains seem to exist, which is also in agreement with the electron microscopic observation [1,3].

The spectral composition image of the 50/50 PC/PSAN blend after plastic deformation, measured along paths perpendicular to drawing, is shown in Fig. 8a. From a comparison of Fig. 8a with Fig. 7a, it follows that the domains are markedly prolonged in the direction of uniaxial deformation, thus resembling parallel furrows. Fig. 8b shows the image of the same plastically deformed sample, as obtained from a similar measurement of a $36 \times 6\ \mu m^2$ rectangle, in 2D representation; from this figure can be seen that the ellipsoids are formed by drawing from the originally approximately isometric domains. The spatial view of the phase structure provided by the spectroscopic technique is in good agreement with electron micrographs.

3.2. Composition of the conjugate phases in microdomains

For quantitative evaluation of the polymer concentrations in the microdomains seen in the Raman composition images and the composition line profiles (Figs. 3–5), the intensity ratios I^{887}/I^{1002} were calibrated using macro-Raman spectra. In the spectra, the baselines were drawn under the bands at 887 cm^{-1} (PC) and 1002 cm^{-1} (PSAN) and the respective areas between the spectral curves and the baselines were determined (see Fig. 2, curve j). The ratios of the integral intensities I^{887}/I^{1002} were then plotted versus the composition of PC/PSAN (0/100, 20/80, 30/70, 40/60, 50/50, 60/40, 70/30 and 80/20), and the reciprocal ratios I^{1002}/I^{887} versus the same series of the composition values for PSAN/PC. The calibration lines intersecting zero were fitted by the least-squares method. The mean slope of these lines, $k = 0.480$, was obtained as the average of these fittings. The blends PC/PSAN can be considered as two-component systems with concentrations c_{PC} and c_{PSAN}, for which $c_{PC} + c_{PSAN} = 1$. Then, the mean concentration composition as obtained by macro-Raman measurement could be calculated

Fig. 4. 3D spectral images of isotropic zones in the PC/PSAN blends of various compositions. PC/PSAN equals: (a) 20/80; (b) 30/70; (c) 40/60; (d) 50/50; (e) 60/40; (f) 70/30; and (g) 80/20. Intensity (the vertical axis) is proportional to the content of PC-c_{PC}, calculated according to Eq. (1) for each measured point of the respective specimen.

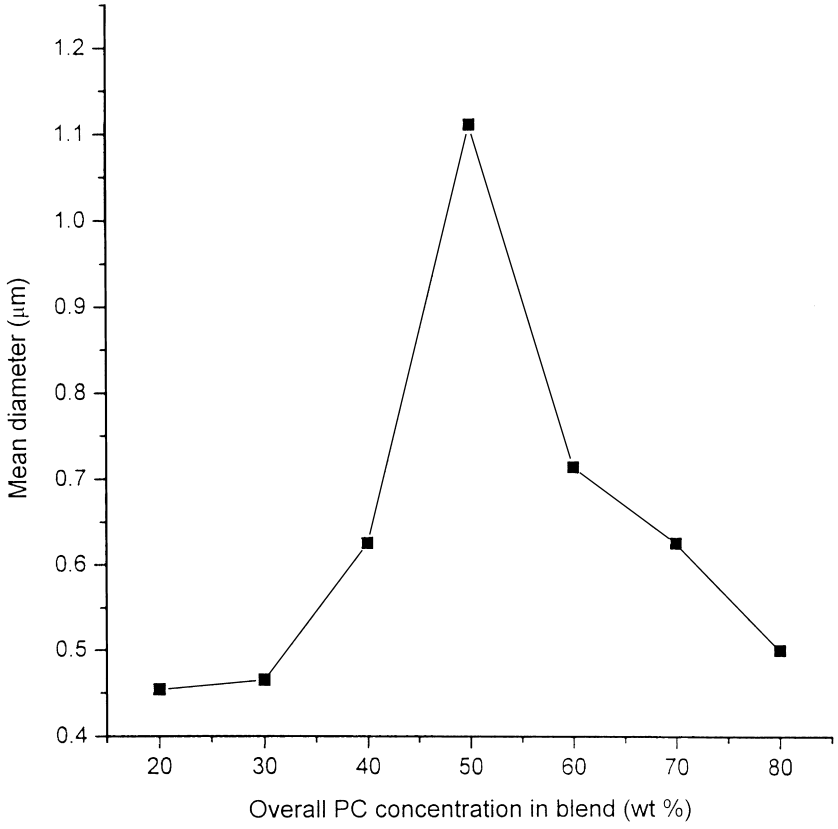

Fig. 6. Mean values of the diameter of PC/PSAN domains for the blends with different overall PC concentrations in blend (wt%).

on the basis of the equation

$$c_{PC} = \frac{I^{887}/I^{1002}}{0.480 + I^{887}/I^{1002}} \quad (1)$$

The experimental points from the macro-Raman measurements located closely around the line with slope 1 in Fig. 9, represent the results of the calculation for the series of the samples with different composition ratio. It follows that the macro-Raman measurements reflect well the mean composition of the PC/PSAN blends.

Whereas the macro-Raman study of our materials reflected the mean values of the concentration composition, the confocal micro-Raman measurement is able to discern the composition of phases in different domains of micron size. The calibration obtained from the macro-Raman spectra was used for the evaluation of the confocal Raman measurements, i.e. for the estimation of the PC concentration in the chosen spectra. Eq. (1) was also employed for the recalculation of the vertical axes of the composition line profiles (Fig. 5) and of the vertical axes in the composition images in the 3D representation (Fig. 4), (primarily constructed by the LABSPEC software as I_{887}/I_{1002} ratios) to correspond to the c_{PC} values.

The maximum and the minimum Raman spectra chosen for each sample from the 400 spectra of the complete spectral image (see Fig. 3) and from the 80 spectra of the measurements of spectral composition line profile, formed the basis for the calculation of the extreme c_{PC} values. The results are shown in Fig. 9. This figure also shows extreme results obtained with the objective magnifying 10×. It is clear that the objective with the highest available 100× magnification yields the largest differences in the concentration values. At the same time, it follows that the confocal Raman measurements give the greatest differences between the maximum and the minimum concentration values for the coarse-grained domains, larger than 2 μm. So, in the case of PC/PSAN = 60/40, the PC-rich and PSAN-rich large domains were found to contain 83 and 16% of PC, respectively. Thus, the direct spectroscopy method yields slightly higher values of partial miscibility in comparison with the indirect results calculated by DSC [1], which gave values 92 and 9% of PC for the same specimen. The difference can be explained by considering that the confocal Raman imaging technique is limited by its confocal spatial resolution, which is ca 1 μm in lateral dimensions and ca 2–3 μm in depth, i.e. the real volumes, even for the largest domains of the dispersed material, are comparable or smaller than the volume which is analysed spectroscopically. Hence, the differences in concentrations found for the largest PC-rich and PSAN-rich domains are underestimated. In the case of smaller domains, the differences evidently are lower than real; for the domains with size <0.5 μm, the concentration images become fully smoothed out and, although the contours of the domains are even here more or less discernible, the correct

concentrations cannot be estimated at all. The maximum and the minimum spectra for each sample (Fig. 3) actually correspond to the largest domains found. The concentration scale given on the perpendicular axes of the concentration line profiles of Fig. 5 and of the images of Fig. 4 is to be understood similarly: it reflects real concentrations sufficiently well only for the largest domains (PC/PSAN = 50/50, 60/40). The smaller the domains, the higher is the apparent concentration of minority components in conjugate phases.

In spite of the limitations described above, confocal micro-Raman imaging spectroscopy can be viewed as a promising technique for the analysis of the phase structure and composition of conjugate phases in polymer blends.

3.3. Molecular orientation and disorientation in PC/PSAN blends

The behaviour of the PC/PSAN blends with respect to the changes in chain orientations occurring during injection moulding and subsequent plastic deformation beyond the yield point was studied. Measurements on different drawn and non-drawn parts of the dumbbells by the polarised visible light showed that the injection-moulded material was partially oriented and that the mean orientation was enhanced by subsequent cold-drawing.

Fig. 10 shows the PA-FTIR spectra of the PC/PSAN cold-drawn specimens of different composition. They were measured with the polariser transmitting the radiation with the electric vector parallel to the direction of drawing. Two systems of IR bands characteristic of the PC and PSAN part of the material from traces (a) and (i) can be identified. Fig. 11 shows the transmittance IR spectra of related thin films of PC/PSAN mixtures evaporated from $CHCl_3$ solution on KBr windows. Comparing Figs. 10 and 11, it follows that the shapes of the strongest PC bands in the PA-FTIR spectra change with blend composition and, in accordance with Ref. [4], their intensities show a non-additive behaviour as a result of the saturation effect. Nevertheless, for the bands of medium or low intensities (not too different for the two polarisations), the photoacoustic spectra are roughly proportional to the concentrations and therefore they can be used for the study of the orientation of PC and of PSAN in the blends [8]. Taking this into account and inspecting the spectra shown in Figs. 10 and 11, the polarised parallel bands at 1080 and 703 cm^{-1} were chosen for the estimation of the orientation of PC and PSAN, respectively.

The analysis of the transition moments of these parallel IR bands, corresponding to PC aromatic in-plane and PSAN aromatic out-of-plane C–H bending vibrations, respectively [9], was used for a more quantitative estimation of polymer orientation. In the specific case of uniaxial orientation, the orientation distribution function obtained by IR spectroscopy is equivalent to the fraction f of the polymer chains perfectly oriented in the stretching direction and is

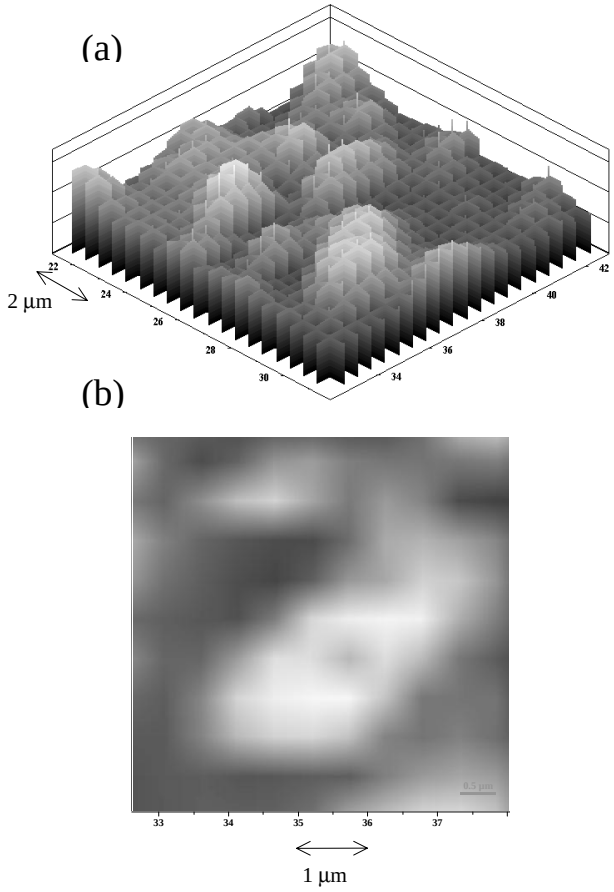

Fig. 7. (a) 3D representation of the spectral image of an isotropic region of 50/50 PC/PSAN blend; intensity (the vertical axis) is proportional to the I^{887}/I^{1002} ratio in the respective point of the specimen; (b) 2D magnified representation of the spectral image of a part of the same region, showing its complex structure; increasing PC/PSAN ratio is represented by increasing whiteness of the picture.

given [10] by

$$f = \frac{D-1}{D+2} \times \frac{2\mathrm{cotg}^2\,\psi + 2}{2\mathrm{cotg}^2\,\psi - 1} \tag{2}$$

where dichroic ratio $D = A_{\parallel}/A_{\perp}$ is the ratio of absorbances for linearly polarised light parallel and perpendicular to the chain direction and ψ is the angle between the transition moment vector and the chain axis. In the case when the exact value of the angle ψ is not known, the expression $(D-1)/(D+2)$ can be considered as a relative orientation function representing the lower limit for f according to Eq. (2).

In amorphous polymers, the angle ψ in Eq. (2) can be approximated by the direction of the transition moment with respect to the local chain axis, and then the overall orientation function f is given by the weighed mean value of orientation functions corresponding to all conformationally different chain segments. In vinyl polymers, the local chain axis is defined as the line joining two adjacent methylene groups [11]. The planes of phenyl rings in PSAN are

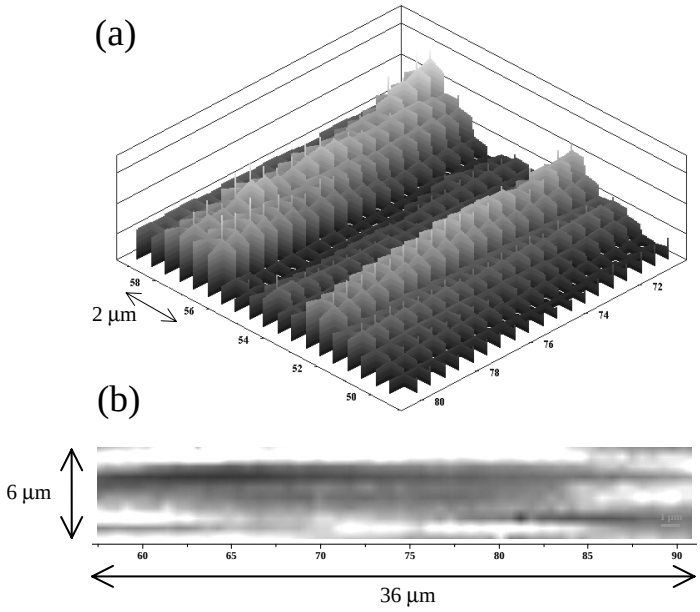

Fig. 8. Spectral image of the 50/50 PC/PSAN blend, a zone after plastic deformation: (a) a 3D representation; intensity (the vertical axis) is proportional to the I^{887}/I^{1002} ratio in the respective point of the specimen; (b) 2D representation of a longer zone, increasing PC/PSAN ratio is represented by increasing whiteness of the picture.

oriented perpendicularly to the local chain direction and, therefore, all the transition moment vectors of the out-of-plane C–H bending vibrations can be expected to be approximately parallel to the chain direction ($\psi \sim 0^{\circ}$), and the orientation function should thus be given directly by the expression $(D-1)/(D+2)$. On the other hand, molecular simulations and experimental evidence indicate [12–16] that in amorphous PC, monomer units with *trans–trans*

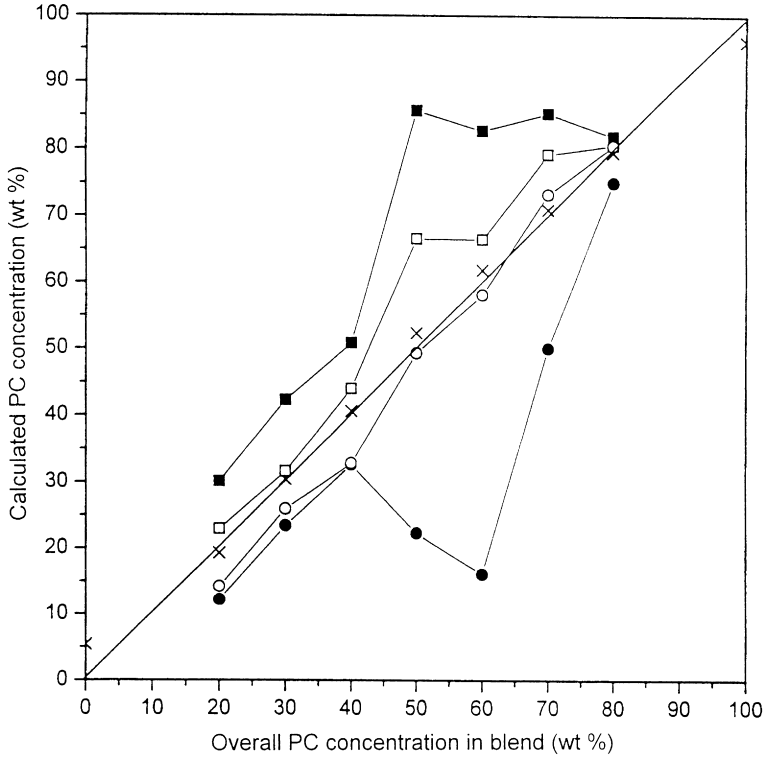

Fig. 9. Concentrations of PC calculated for the specimens of different overall PC concentrations in blend (wt%) from: (a) the spectra of macro-Raman measurements (×); (b) the spectra with the maximum intensities of PC-band (□) and of PSAN-band (○) found among 80 measurements with the objective 10×; (c) the spectra with maximum intensities of PC-band (■) and of PSAN-band (●) found among 480 measurements with the objective 100×.

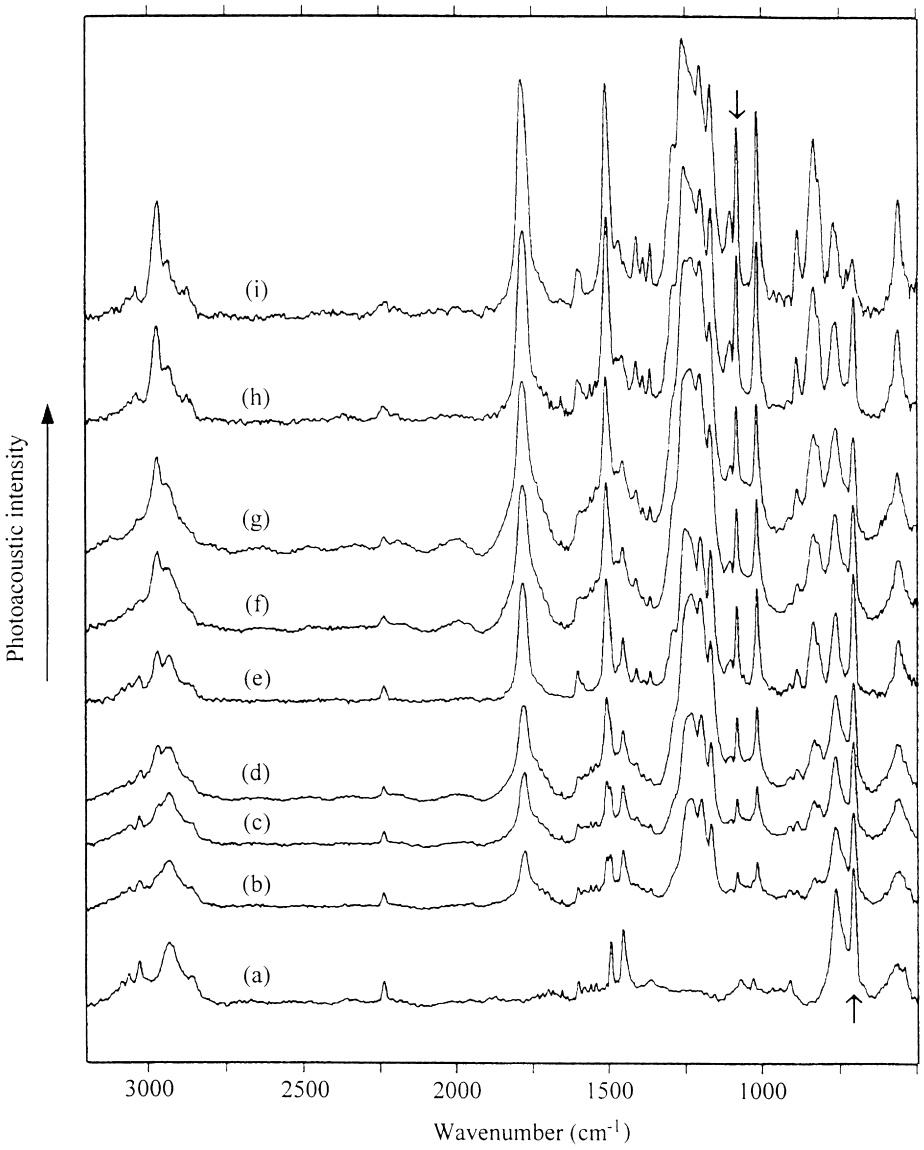

Fig. 10. Normalized PA-FTIR spectra of plastically cold-drawn PC/PSAN specimens. PC/PSAN equals: (a) 0/100; (b) 20/80; (c) 30/70; (d) 40/60; (e) 50/50; (f) 60/40; (g) 70/30; (h) 80/20; and (i) 100/0. (Electric vector parallel the cold-drawing direction.)

and *cis–trans* conformational forms of carbonate groups and, consequently, chain segments with various local conformational structures are present. In Fig. 12, three types of PC chain segments are shown, with banana shape *tt–tt* and approximately linear *tc–tc* and *tc–ct* conformational sequences [17]. Directions of the transition moment vectors in PC have been predicted using ab initio calculations of the normal modes for model compounds. According to the calculations for $(CH_3)_3C–(1,4\text{-}C_6H_4)–O–(CO)–CH_3$ at the B3LYP/6-31G(d) level, the transition moment of the aromatic in-plane C–H bending (calculated frequency 1039 cm^{-1}) is only slightly deviated from the phenyl axis (2.4°). Therefore, the angle ψ and the corresponding factor $(2\cot g^2\ \psi + 2)/(2\cot g^2\ \psi - 1)$ can be estimated from the direction of the phenyl axis with respect to the local chain axes. For the PC sequences given in Fig. 12, the angles ψ are 35° (*tt–tt*), 25 and 45° (*tc–tc*) and 35° (*tc–ct*). Therefore, to obtain orientation functions, the values $(D - 1)/(D + 2)$ in Table 1 have to be multiplied by a factor 2.0–2.7, depending on the populations of conformational sequences.

The actual final orientation levels of the cold-drawn PC and PC/PSAN samples depend individually on specific conditions of drawing. In our PC/PSAN samples from 100/0 to 40/60, the achieved chain orientation was between 0.25 and 0.70. PA-FTIR spectra of a cold-drawn specimen of the PC/PSAN 50/50 blend along with the spectra of the same sample annealed for 20 h at temperatures of 80, 115 or 150°C, measured with two mutually perpendicular orientations of the polariser, are shown in Fig. 13; the corresponding values of the chain orientations can be found in Table 1. As can be seen from Fig. 13; curves (a) and from Table 1, the 50/50 PC/PSAN blend is partially oriented by plastic

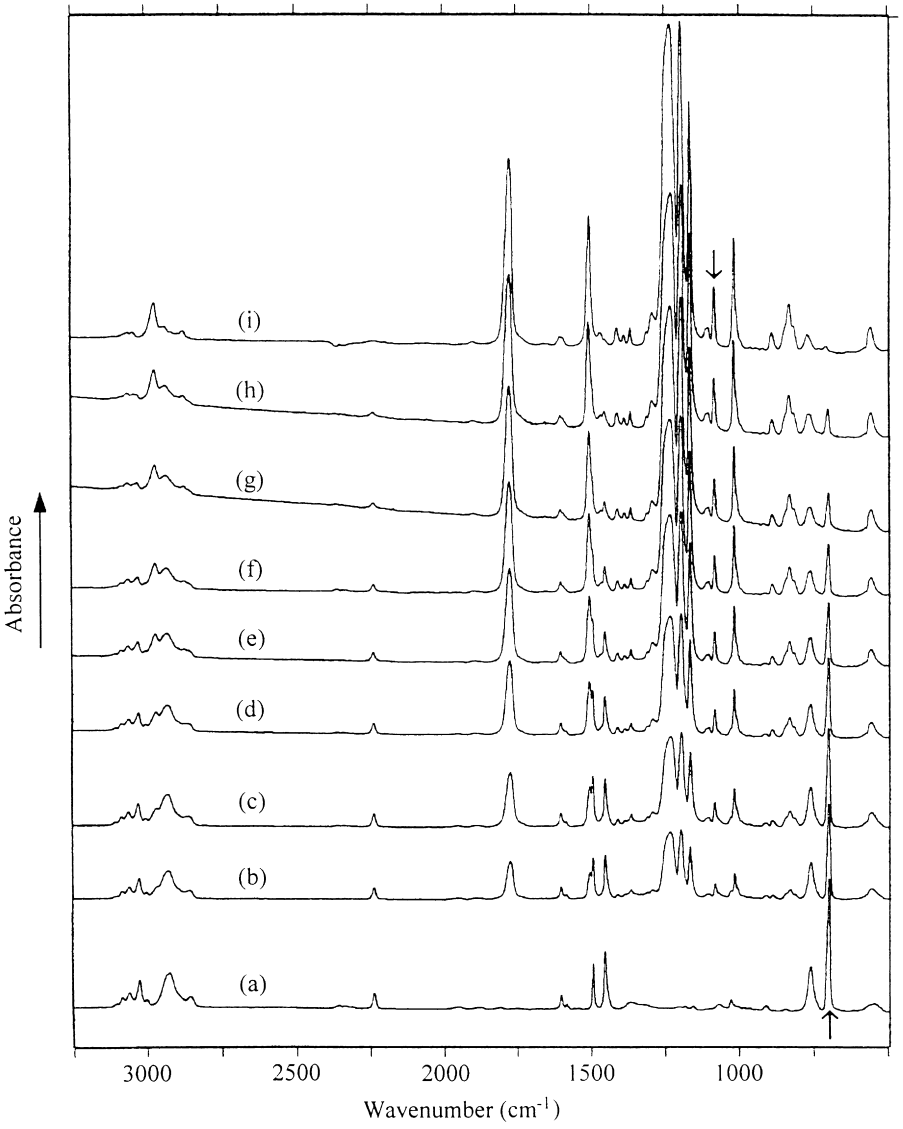

Fig. 11. Comparative unpolarised normalized FTIR transmittance spectra of PC/PSAN films evaporated from $CHCl_3$ solution on KBr windows. PC/PSAN equals: (a) 0/100; (b) 20/80; (c) 30/70; (d) 40/60; (e) 50/50; (f) 60/40; (g) 70/30; (h) 80/20; and (i) 100/0.

deformation. From the above consideration and from the results in Table 1, it follows that during the injection-moulding and the subsequent cold-drawing, PC in the PC/PSAN = 50/50 blend can reach quite a substantial degree of orientation. On the other hand, PSAN, which can be cold-drawn only as a part of the blend, reaches in the 50/50 specimen only a small value of the orientation function.

After annealing the material, the differences between the band intensities in the two measurements with mutually perpendicular polarised light diminish; the related relative orientations, expressed as the percentage of the corresponding values before annealing, thus indicate gradual disorientation of the material (see Fig. 13 and Table 1). At the temperature of 115°C, i.e. above the glass transition temperature of PSAN (~105°C) but below the glass transition temperature of PC (~150°C), the polarised intensities of the 703 cm^{-1} band (assigned to the out-of-plane vibration of the styrene aromatic rings) become nearly equal. The majority of the PSAN component in this blend material was disoriented during the annealing, whereas the partial orientation of the PC component reflected in the 1080 cm^{-1} band still persisted. Generally, the PC parts of the blend are more resistant to annealing. Heating at 150°C equalised the intensities in the whole spectra of opposite polarisation—the material was completely disoriented after annealing at that temperature.

Owing to very good interfacial adhesion in the PC/PSAN blends, the plastic deformation of both conjugate phases proceeds simultaneously. On the other hand, the orientation of PC chains is much higher than that of the PSAN chains. The latter effect can be attributed to a high flexibility of the PC backbone, whereas the PSAN chains are rather stiff [18].

From a comparison of the dichroism of the PC aromatic 1080 cm^{-1} band with the band of the carbonyl vibration,

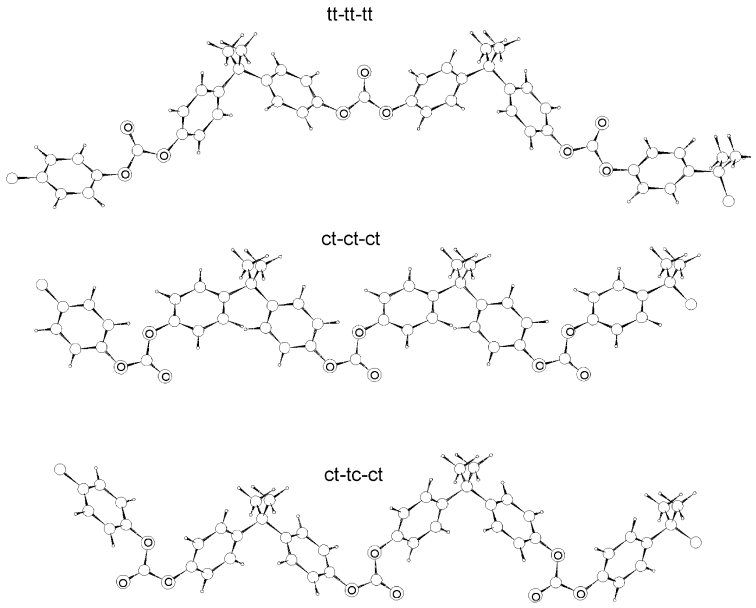

Fig. 12. Chain segments of PC with *tt–tt*, *tc–tc* and *tc–ct* conformational structures of the carbonate groups.

another conclusion concerning the conformation of the PC chain follows. According to the normal mode calculations of diphenyl carbonate at the B3LYP/6-31G(d) level, the transition moment of the carbonyl stretching vibration in the *trans–trans* conformational structure is exactly parallel to the C=O direction, and thus the corresponding transition moment in the *tt–tt* sequence of PC should be perpendicular to the local chain axis (Fig. 12). In the *trans–cis* structure of diphenyl carbonate, the transition moment of the carbonyl stretching is deviated by 2.5° from the C=O bond towards the phenyl group in the *cis* position. Based on these results, the corresponding angles ψ of transition moments with respect to the local chain axes in the *tc–tc* and *tc–ct* sequences of PC (Fig. 12) are approximately 40 and 30°, respectively, and the carbonyl bands originating from these sequences should exhibit parallel dichroism. It can be seen in Fig. 13 curves a, that for cold-drawn samples, which are substantially oriented according to the f^{1080} orientation function (Table 1), carbonyl bands of PC at 1780 cm^{-1} show negligible dichroism. This indicates that a relatively high portion of the *tc–tc* and *tc–ct* segments with parallel polarised C=O stretching vibrations must be present in amorphous PC to compensate for the perpendicular dichroism of the C=O stretching in *tt–tt* structures. With respect to the on-going discussion concerning the content of different carbonate conformations in amorphous PC, this supports indications of molecular simulations [13,14] and of a recent vibrational spectroscopy study [12] that the content of the *cis–trans* structure is higher than that estimated from NMR experiments [16].

4. Conclusions

1. In partially miscible PC/PSAN blends, the PC-rich and PSAN-rich domains were identified by the confocal Raman imaging spectroscopy. This method simultaneously provides information on
   1.1. phase structure, which is coarser for the blends with comparable contents of both components and finer for the blends where one component prevails. Original isometric domains are transformed into elongated ellipsoids by plastic deformation. Phase structure contours revealed by the spectroscopic

Table 1
Molecular orientation in PC/PSAN = 50/50 blend

Annealing temperature (°C)	PC					PSAN			
	D^{1780}	D^{1080}	$\frac{D^{1080}-1}{D^{1080}+2}$	f^{1080}	Relative orientation of PC (%)	D^{703}	$\frac{D^{703}-1}{D^{703}+2}$	f^{703}	Relative orientation of PSAN (%)
Not annealed	0.9	1.65	0.18	0.36–0.49	100	1.20	0.06	0.06	100
80	0.9	1.65	0.18	0.36–0.49	100	1.11	0.03	0.03	62
115	1.0	1.43	0.12	0.24–0.32	87	1.02	0.01	0.01	<13
150	1.0	~1.0	0.0	0.0	0	~1.0	0.0	0.0	0

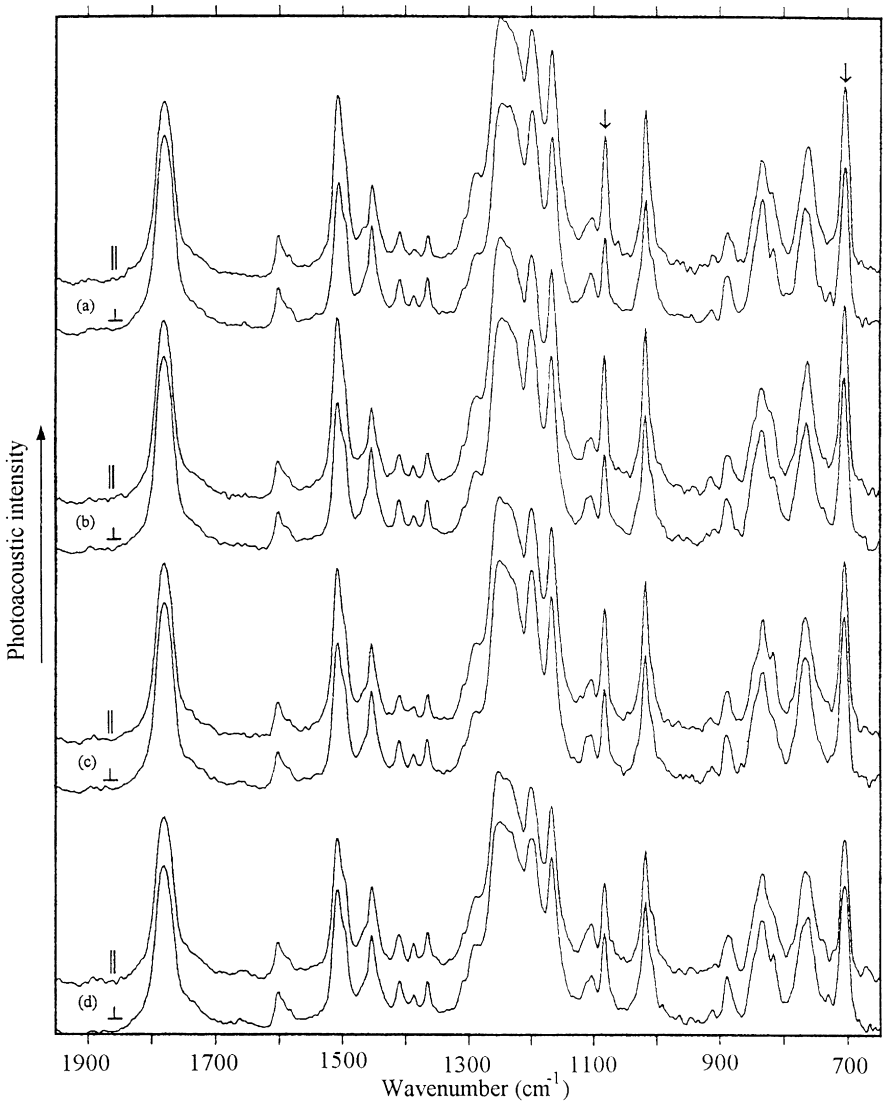

Fig. 13. PA-FTIR spectra of cold-drawn 50/50 PC/PSAN blends polarised in parallel (∥) and perpendicular (⊥) direction to the cold-drawing (a) without annealing, and after annealing at (b) 80; (c) 115; and (d) 150°C.

technique are in good agreement with those obtained by electron microscopy.

1.2. the local composition of conjugate phases in individual large PC-rich and PSAN-rich domains, which was for the first time obtained by a direct spectroscopic method. These results are in conformity with those calculated from collective T_g measurements [1].

2. The chain orientation of PC/PSAN blends attained during plastic deformation of specimens up to fracture was estimated by PA-FTIR with polarised radiation. The PC chains in the blends are substantially oriented in the process of plastic deformation; on the other hand, PSAN, despite marked elongation of the microdomains, attains only a slight chain orientation. On annealing at temperatures between the glass transitions of the components, the disorientation of the chains of each blend component proceeds independently. Comparison of the dichroisms of the bands assigned to C=O stretching and aromatic in-plane C–H bending indicates high contents of the *cis–trans* conformation of the carbonate group in amorphous PC.

Acknowledgements

The authors are greatly indebted to the Grant Agency of the Czech Republic (Grants No. 106/97/1071 and 203/97/0539) and to the Grant Agency of the Academy of Sciences of the Czech Republic (Grant no. A4050706) for financial support. Thanks are also given to Dr K.J. Eichhorn, Institute of Polymer Research, Dresden, Germany, who enabled us to measure the PA-FTIR spectra in his laboratory.

References

[1] Kolařík J, Lednický F, Pegoraro M. Polym Networks Blends 1993;3:147.
[2] Lednický F, Hromádková J, Kolařík J. Polym Test 1999;18:123.
[3] Kolařík J, Lednický F, Locati GC, Fambri L. Polym Eng Sci 1997;37:128.
[4] Quintanilla L, Rodriguez-Cabello JC, Jawhari T, Pastor JM. Polymer 1994;35:514.
[5] Schmidt P, Fernandez MR, Pastor JM, Roda J. Polymer 1997;38:2067.
[6] Dhamelincourt P, Barbillat J, Delhaye M. Spectrosc Eur 1993;5(2):l6.
[7] Williams KPJ, Batchelder DN. Spectrosc Eur 1994;6(1):19.
[8] Schmidt P, Raab M, Kolařík J, Eichhorn KJ. Polym Test 2000; in press.
[9] Socrates G. Infrared characteristic group frequencies, New York: Wiley, 1980. p. 83.
[10] Fraser RDB. J Chem Phys 1958;29:1428.
[11] Jasse B, Oultache AK, Mounach H, Halary JL, Monnerie L. J Polym Sci Part B: Polym Phys 1996;34:2007.
[12] Dybal J, Schmidt P, Baldrian J, Kratochvíl J. Macromolecules 1998;31:6611.
[13] Williams AD, Flory PJ. J Polym Sci: Polym Phys Ed 1968;6:1945.
[14] Hutnik M, Argon AS, Suter UW. Macromolecules 1991;24:5956.
[15] Hutnik M, Gentile FT, Ludovice PJ, Suter UW, Argon AS. Macromolecules 1991;24:5962.
[16] Tomaselli M, Zehnder MM, Robyr P, Grob-Pisano C, Ernst RR, Suter UW. Macromolecules 1997;30:3579.
[17] Červinka L, Fischer EW, Dettenmaier M. Polymer 1991;32:12.
[18] Wu S. Polym Int 1992;29:229.